1981ApJ...250...66V

THE ASTROPHYSICAL JOURNAL, 250:66–78, 1981 November 1
© 1981. The American Astronomical Society. All rights reserved. Printed in U.S.A.

ORBITAL MOTION OF THE HEAD-TAIL RADIO GALAXY IC 708

J. P. VALLÉE[1]
Department of Physics, Queen's University at Kingston, Ontario
A. H. BRIDLE[2]
National Radio Astronomy Observatory[3] VLA Program and
Department of Physics and Astronomy, University of New Mexico
AND
A. S. WILSON
Astronomy Program, University of Maryland
Received 1981 February 25; accepted 1981 May 4

ABSTRACT

The Very Large Array has been used to map the unusual head-tail radio galaxy IC 708 in the cluster of galaxies Abell 1314 with resolutions from 0".5 to ~ 3".3 at 4.89 GHz. The new data strongly suggest that the unusual structure of the source is due to a gravitational interaction between IC 708 and its neighbor IC 709 while both orbit the center of Abell 1314.

The shapes of the radio trails and some details of the variation of intensity along them can be explained by projection effects arising from the orbital motion of IC 708 and by the effects of the variation of the orbital velocity of IC 708 on the motions of its ejecta. We have made numerical simulations of the orbiting head-tail system incorporating various models of the ejecta dynamics. The most satisfactory model for the structure is one in which a pair of continuous supersonic jets bends behind IC 708 under the ram pressure of the intracluster medium. Furthermore, the distributions of intensity and polarization over the trails of IC 708 resemble those observed in straight radio jets in several low luminosity radio galaxies. It appears that external pressures have bent similar jets in IC 708 through almost 90° without disrupting them.

Subject headings: galaxies: individual — galaxies: structure — radio sources: galaxies

I. INTRODUCTION

The head-tail radio galaxies which have been mapped at high resolution and at many frequencies have been used both as probes of the intracluster medium (ICM) in clusters of galaxies (e.g. Jaffe and Perola 1973; Miley, Wellington, and van der Laan 1975; Ekers *et al.* 1978) and as test beds for theories of energy transfer and particle acceleration in extended extragalactic radio sources (e.g. Begelman, Rees, and Blandford 1979; Burns, Owen, and Rudnick 1979). Our knowledge of the head-tail structures has recently been reviewed by Miley (1980) and by Vallée (1977).

Table 1 lists the published observations of the head-tail radio galaxy IC 708 ($m_V = 14^m.4$, $z = 0.0320$) in the (richness 0) cluster of galaxies Abell 1314. IC 708 is unique among the known head-tails because at a resolution of ~ 6" (Vallée, Wilson, and van der Laan 1979) its twin trails of radio emission appear to flare outwards into diffuse "wings" of emission some 35 kpc ($H_0 = 50$ km s^{-1} Mpc^{-1}) from the center of the optical galaxy. This curious morphology motivated the description of IC 708 as a "papillon" ("butterfly") structure by Vallée, Wilson, and van der Laan (1979), who interpreted the structure in terms of the dynamical effects of a hypothetical thermal pressure gradient downstream of IC 708. Such a gradient might be caused by accretion of the ICM behind IC 708 in its orbit (e.g., Hunt 1971, 1979) or by ablation of the gas lost by stars in IC 708 under the ram pressure of the ICM (e.g., Gisler 1976; Lea and De Young 1976).

Section II of this paper presents new 4.89 GHz observations of IC 708 made with the partially completed VLA (Thompson *et al.* 1980). These observations provide the highest resolution maps so far available of IC 708. The new maps suggest an alternative interpretation of its structure in terms of gravitational interactions between IC 708, its close neighbor IC 709, and the center of mass of Abell 1314. The basis of this new interpretation is outlined in § III. Section IV describes an approach used to make numerical models of the radio trail structure of IC 708, and § V discusses the consequences of these models for the physical parameters of the radio trails. Throughout the paper we adopt a Hubble parameter $H_0 = 50$ km s^{-1} Mpc^{-1} and a deceleration parameter $q_0 = 0.5$.

II. THE VLA OBSERVATIONS

The new 4.89 GHz observations were made in 1979 February with 14 VLA antennas. Important parameters of the observations are listed in Table 2. All available

[1] Now at Herzberg Institute of Astrophysics, Ottawa.
[2] On leave from Queen's University at Kingston.
[3] The National Radio Astronomy Observatory is operated by Associated Universities Inc., under contract with the National Science Foundation.

© American Astronomical Society • Provided by the NASA Astrophysics Data System

1981ApJ...250...66V

TABLE 1

OBSERVATIONS OF IC 708 WITH HPBW LESS THAN 5 ARC MIN

Wavelength (cm)	Mapped Flux Density (Jy)	Highest Resolution (arcsec)	Telescope	Reference
49.2	1.43	52 × 69	Westerbork	Vallée and Wilson 1976
21.2	0.84	23 × 30	Westerbork	Wilson and Vallée 1977
11.1	0.52	9 × 13	NRAO 3-element Interferometer	Owen and Rudnick 1976
11.1	0.63[a]	276 × 276	Bonn 100 m	Haslem *et al.* 1978
6.1	0.28[b]	0.5 × 0.6	VLA	This paper
6.0	...	6 × 8	Westerbork	Vallée and Wilson 1976
6.0	0.38	6 × 8	Westerbork	Vallée *et al.* 1979
3.7	0.08[c]	3 × 4	NRAO 3-element Interferometer	Owen and Rudnick 1976

[a] May be contaminated by emission from nearby galaxy IC 711.
[b] In structure unresolved by shortest spacing of 90 m.
[c] In structure unresolved by shortest spacing of 100 m.

antenna pairs and polarizations were correlated, giving 91 baselines ranging from 90 m to ~ 18 km. The intensity scale was normalized to an assumed flux density for 3C 286 of 7.41 Jy at 4.89 GHz. The instrumental polarization was calibrated by observing 3C 286 for 55 minutes near its meridian crossing, using an 80° rotation of the parallactic angle with respect to the altazimuth antennas. We assumed 3C 286 to be 11% linearly polarized with the *E*-vector at p.a. 33° when normalizing the polarization position angles.

Maps of the distribution of the Stokes parameters I, Q, and U were produced from the calibrated visibility data by the usual Fourier methods. Sidelobe responses resulting from nonuniform coverage of the (u, v) plane were deconvolved from the maps using a CLEAN algorithm (Högbom 1974). The Q and U maps were combined to obtain the distributions of the total linearly-polarized intensity $(Q^2 + U^2)^{1/2}$ and of the *E*-vector position angle $\chi = \frac{1}{2} \arctan (U/Q)$.

a) Map at ~ 0″.5 Resolution

Figure 1 shows the CLEANed map of total intensity (Stokes I) within ~ 5″ (4.4 kpc) of the optical nucleus of the galaxy, at an angular resolution of 0″.51 by 0″.63 (major axis in p.a. 140°). An unresolved (< 0″.2) radio core with flux density 49 ± 1 mJy coincides to within the uncertainties with the optical centroid of the galaxy. (The radio core position is $\alpha(1950.0) = 11^h31^m16^s.25 \pm 0^s.01$, $\delta(1950.0) = +49°20'18''.1 \pm 0''.1$, and the optical centroid (Vallée and Wilson 1976) is at $\alpha(1950.0) = 11^h31^m16^s.36 \pm 0^s.1$, $\delta(1950.0) = +49°20'18''.1 \pm 1''$). At this angular resolution the extended emission is dominated by a one-sided linear "jet"-like feature ~ 4 kpc in length emanating from the nucleus of the galaxy in p.a. 10° ± 2°. The length of this feature is similar (1) to those of the bright one-sided bases of the long two-sided radio jets in 3C 31 and NGC 315 (Fomalont *et al.* 1980), (2) to those of the radio and optical jets in M87 (Turland 1975;

TABLE 2

PARAMETERS OF THE VLA OBSERVATIONS

Field center:			
α (1950.0)	$11^h31^m14^s.0$		
δ (1950.0)	+49°20′30″.0		
Observing date	1979 February 3		
Observing frequency (wavelength)	4.885 GHz (6.1 cm)		
Nominal system temperature	50 K		
Bandwidth	50 MHz		
Secondary calibration source: 1216+487 (0.99 Jy)	$12^h16^m38^s.6$, +48°46′35″		
Source scan duration, calibrator scan duration	12 min, 3 min		
Hour angle coverage	$-7^h.0$ to $+8^h.1$		
Antenna configuration:	Southeast Arm	Southwest Arm	North Arm
Azimuth of arm	114°59′42″	236°00′03″	354°59′42″
Antenna locations	−80.00 m	484.01 m	436.41 m[a]
	+89.91 m[a]	1589.91 m[a]	
	483.98 m[a]	3188.10 m[a]	
	970.46 m[a]	7659.46 m[a]	
	1589.89 m[a]	10472.84 m	
	1946.01 m[a]	13643.90 m[a]	
		17157.20 m[a]	

[a] Antennas used for Stokes Q and U, as well as I.

© American Astronomical Society • Provided by the NASA Astrophysics Data System

1981ApJ...250...66V

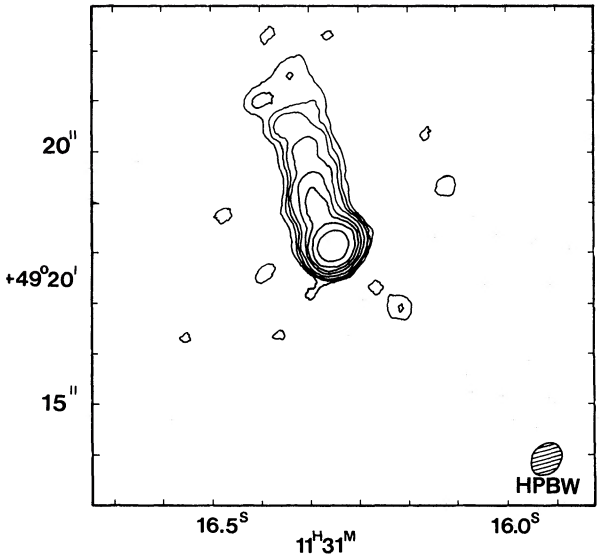

FIG. 1.—4.89 GHz brightness distribution over IC 708 with resolution 0".51 by 0".63 (major axis in p.a. 140°). Contours are drawn at 2%, 3%, 4%, 6%, 10%, 15%, 25%, and 50% of the peak of 49 mJy per beam. The FWHM of the synthesized beam is indicated by the shaded ellipse.

Owen, Hardee, and Bignell 1980; de Vaucouleurs and Nieto (1979), and (3) to those of several one-sided jets found in quasars by VLBI mapping (Wilkinson *et al.* 1977; Readhead *et al.* 1979). No counterjet is detected at this resolution.

At the resolution of this map, the position angle χ of the E-vector of the linear polarization is aligned roughly perpendicular to the jet from the radio core up to 2" (1.8 kpc) along the jet, where the polarized intensity decreases to the rms noise of about 0.3 mJy per beam area. The percentage of linear polarization, $p = 100(Q^2 + U^2)^{1/2}/I$, increases from about 1% at the radio core to about 10% at 1".33 (1.2 kpc) along the jet.

b) Map at ~ 1".3 Resolution

Figure 2 shows the CLEANed map at 1".3 by 1".4 resolution (major axis in p.a. 35°) obtained by tapering the observed visibility amplitudes with a Gaussian function falling to $1/(e)^{1/2}$ at 5 km from the center of the (u, v) plane. At this resolution the "jet"-like feature of Figure 1 blends into an arclike or **U**-shaped structure whose apex is at the unresolved radio core. As depicted in Figure 2, the bending occurs well within the 30" overexposed central region of the image of IC 708 on the red-sensitive Palomar Sky Atlas print. This emission arc appears to have structure on a scale of about 4" (3.5 kpc), reminiscent of that found in NGC 1265 at 6 cm by Owen, Burns, and Rudnick (1978).

c) Map at ~ 3".3 Resolution

Figure 3 shows the CLEANed total intensity map at 3".3 by 3".9 resolution (major axis in p.a. 24°) obtained by applying a 2 km Gaussian taper to the observed visibility amplitudes. This map has better sensitivity to the large scale structure of the radio trails. The two "flares" at the western ends of the trails observed at 6" by 8" resolution by Vallée, Wilson, and van der Laan (1979) are each resolved on this map into a "hook" structure. This hook structure can also be seen on the map at ~ 1".3 resolution in that area, although the signal-to-noise is poorer in that map. Both trails contain substructure on a scale of about 6" (5 kpc). Their widths slowly increase with distance from the galaxy, from 7" (6.2 kpc) between 24" and 80" (21 and 70 kpc) from IC 708 to 13" (11.5 kpc) at 95" (84 kpc) from the galaxy and 15" (13 kpc) beyond 100" (88 kpc).

As the shortest baseline in the VLA observations was 90 m, 28% of the total intensity in the 6 cm WSRT map (Vallée, Wilson, and van der Laan 1979) is missing from our maps. A comparison with the WSRT map shows that this missing intensity would partly fill the regions within the two "hooks" in Figure 3.

d) Polarization and Magnetic Field Configuration

Figure 4 shows the large scale distribution of the E-vector of the linear polarization at the resolution of Figure 3. The polarized signal is weak, but its distribution agrees well with that found by Vallée, Wilson, and van der Laan (1979) after allowing for their lower resolution. The E-vectors are roughly parallel to the lengths of the radio trails between 8" (7.0 kpc) and 50" (44 kpc) from the radio core. Further from the core, where the ridges begin to turn

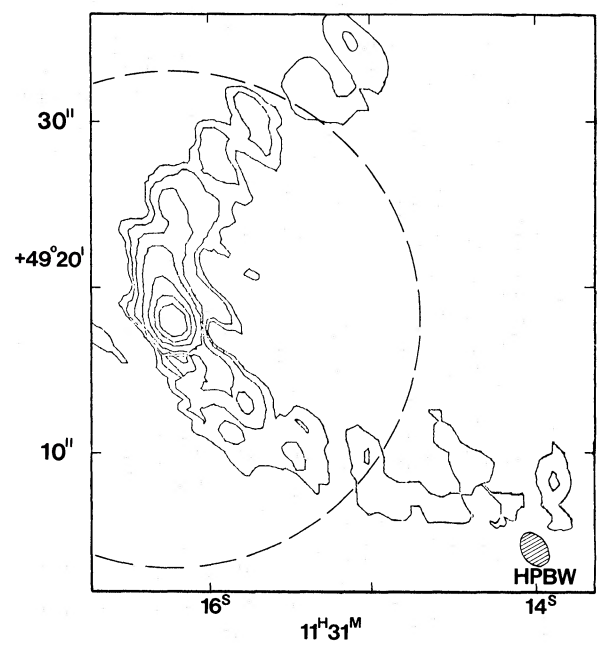

FIG. 2.—4.89 GHz brightness distribution over IC 708 with resolution 1".3 by 1".4 (major axis in p.a. 35°). Contours are drawn at 0.75%, 1.5%, 3%, 6%, 15%, 30%, and 50% of the peak of 59 mJy per beam. The FWHM of the synthesized beam is indicated by the shaded ellipse. The dashed curve depicts the boundary of the overexposed core of IC 708 on the red print of the Palomar Sky Atlas.

© American Astronomical Society • Provided by the NASA Astrophysics Data System

1981ApJ...250...66V

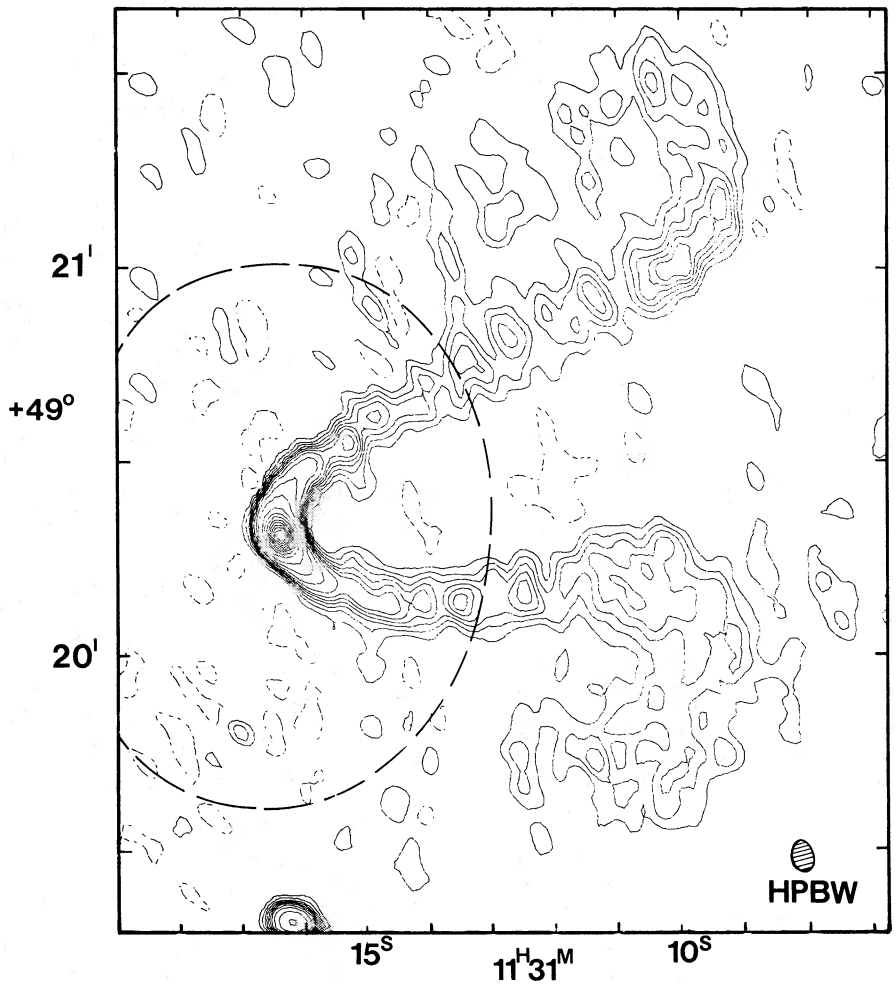

FIG. 3.—4.89 GHz brightness distribution over IC 708 with resolution 3″.3 by 3″.9 (major axis in p.a. 24°). Contours are drawn at −0.4%, 0.4%, 0.8%, 1.2%, 1.6%, 2%, 2.4%, 3%, 4%, 6%, 10%, 20%, 30%, 40%, 50%, 60%, 70%, 80%, and 90% of the peak of 78 mJy per beam. The FWHM of the synthesized beam is indicated by the shaded ellipse. The dashed curve depicts the boundary of the envelope of IC 708 on the red print of the Palomar Sky Atlas.

to form the hooked structures, the *E*-vectors turn, becoming inclined at $\sim -45°$ to the line of the northern ridge and at $\sim +45°$ to the line of the southern. The percentage of linear polarization varies from about 40% at 15″ (13 kpc) from the radio core to < 20% at 50″ (44 kpc) from the core and about 35% at 70″ (62 kpc) from the core.

As the 1.4–5 GHz Faraday rotation measure along both radio trails is known to be -20 ± 20 rad m^{-2} from the WSRT data, the observed 4.89 GHz *E*-vectors should be within $\sim 5°$ of their intrinsic (zero wavelength) orientations over most of this structure. The dominant component of the magnetic field in the trails must therefore be *perpendicular* to their length for most of the 50 kpc distance from the radio core to the hooks (excluding the first few kpc, where the field lies mainly *parallel* to the jetlike feature in Figure 1). This magnetic configuration is the same as that in several straight two-sided radio jets with similar linear scales and radio luminosities (e.g., those in 3C 449 [Perley, Willis, and Scott 1979] and in 3C 31 and NGC 315 [Fomalont *et al.* 1980]). In particular, the first $\sim$ 5 kpc of the jets in 3C 31 and NGC 315 contain bright one-sided "bases" in which the dominant magnetic field component lies parallel to the jets. Both the one-sidedness of the jetlike feature in Figure 1 and its field configuration resemble those of the "base" regions of these straight radio jets. We cannot however be sure of the magnetic configuration between 2 and 7 kpc from the radio core in IC 708 because there the polarized intensities are too close to the rms noise in our maps.

e) The Source 1131+493B

The compact radio source 1131+493B at 1950.0 position $11^h31^m16^s.1$, +49°19′19″ (roughly 1′ south of the center of IC 708 at the lower edge of Fig. 3) was discussed by Vallée and Wilson (1976) and by Wilson and Vallée (1977), who found that (1) there is no radio connection with the extended structure of IC 708, (2) no optical

© American Astronomical Society • Provided by the NASA Astrophysics Data System

1981ApJ...250...66V

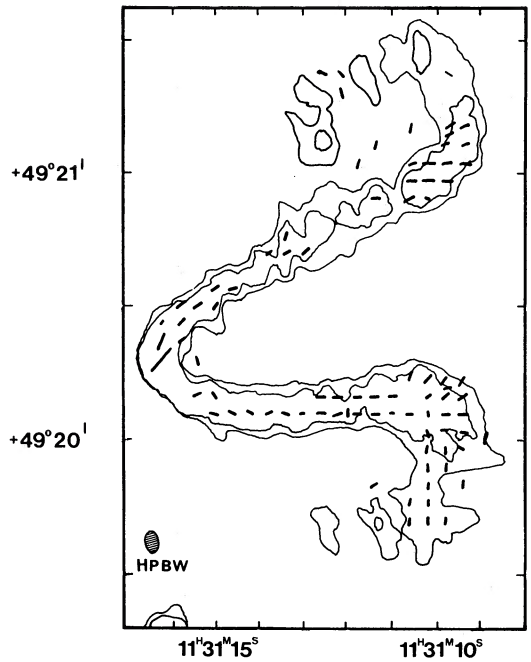

FIG. 4.—Intensity and position angle of linearly-polarized emission from IC 708 at the resolution of Fig. 3. Each vector has a length proportional to the polarized intensity $(Q^2 + U^2)^{1/2}$ and a position angle equal to that of the observed E-vector. The maximum polarized intensity plotted is 2.6 mJy per beam. Outer contours of Fig. 3 are shown for reference.

identification is apparent on the Palomar Sky Atlas prints, (3) its percentage of linear polarization is $< 3\%$, and (4) its spectral index $\alpha \sim 0.65$ $[S(\nu) \propto \nu^{-\alpha}]$ between 1.4 and 5.0 GHz. Our VLA data at $\sim 0''.5$ resolution show the source to be double with a component separation of 1″ in p.a. $\sim 85°$. It is probably a background source unrelated to Abell 1314.

III. THE BASIS OF AN ORBITAL INTERPRETATION OF THE STRUCTURE

The most interesting large scale feature revealed by the new VLA maps of IC 708 is the striking "double-hooked" morphology of the source (Fig. 3). As the twin trail structure within 50 kpc of the center of the galaxy can clearly be explained by the conventional radio "head-tail" hypotheses (e.g. Miley *et al.* 1972), it is natural to retain these while seeking an explanation for the hooked shapes of the ends of the trails. Our basic proposal is that IC 708 has followed a curved trajectory through Abell 1314, with our line of sight lying almost in the plane of the orbit. Superposed on this motion is the usual increase in separation between the two trails characteristic of twin head-tail galaxies such as NGC 1265 (Owen, Burns, and Rudnick 1978). Figure 5 illustrates the basis of such a model for the radio structure.

Orbital interpretations for curvature in head-tail sources with *single* radio trails have previously been proposed, in varying amounts of detail, for 3C 129 (Miley *et al.* 1972; Byrd and Valtonen 1978) and for NGC 4874

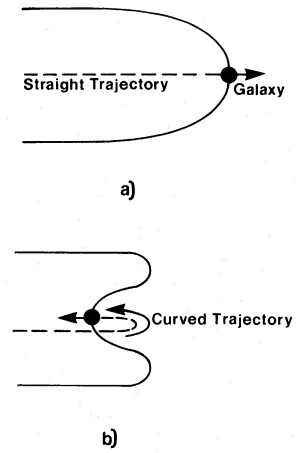

FIG. 5.—Schematic illustration of the basis of orbital models for the trail structure of IC 708. (*a*) The planar twin-trail structure of a head-tail galaxy traveling in a straight line at constant velocity. (*b*) The same structure in the case of orbital motion of the galaxy around a neighboring mass center.

(Jaffe, Perola, and Valentijn 1976; Valtonen and Byrd 1979). In the case of IC 708, the fact that the trail is *double* allows us to match many physical characteristics of the observed structure by varying the parameters of an orbital model, once the center of gravitational attraction for the orbit has been identified.

To begin this identification, we note that the plane of the past orbit of IC 708 must be indicated approximately by the bisector of the two radio trails. The dominant attracting center should therefore be located eastwards from IC 708 along position angle $\sim 108°$. Figure 6 shows the optical field of IC 708 in the central area of Abell 1314.

a) IC 709 as the Attracting Center

We believe that the 15 mag galaxy IC 709 is primarily responsible for the distortions of the radio trails of IC 708 for four reasons. First, as shown in Figure 6, IC 709 is the brightest galaxy in the immediate field near the bisector of the double radio trail of IC 708. Second, IC 709 is only 165″ (145 kpc) in projected separation from IC 708. Third, IC 709 is only 0.8 mag fainter than IC 708 (Zwicky and Herzog 1966), so it should have sufficient mass to deflect IC 708 significantly. Fourth, the IC 708/709 pair is kinematically isolated in Abell 1314: the radial velocities of the two galaxies differ by only 64 ± 210 km s^{-1} from each other but by 568 km s^{-1} from the mean radial velocity of 16 cluster galaxies measured by Coleman *et al.* (1976). Assuming the radial velocities to be Gaussian distributed with a standard deviation of 708 km s^{-1} (Coleman *et al.* 1976), this apparent isolation has only a 5.0% probability of being due to chance. We therefore attempted initially to find "single-orbit" models for the radio structure of IC 708, based on the assumption that IC708 orbits IC 709 alone.

b) Initial Values for Single-Orbit Parameters

In this subsection we obtain *rough* values for the orbital parameters of the IC 708/709 pair. These were used as

© American Astronomical Society • Provided by the NASA Astrophysics Data System

1981ApJ...250...66V

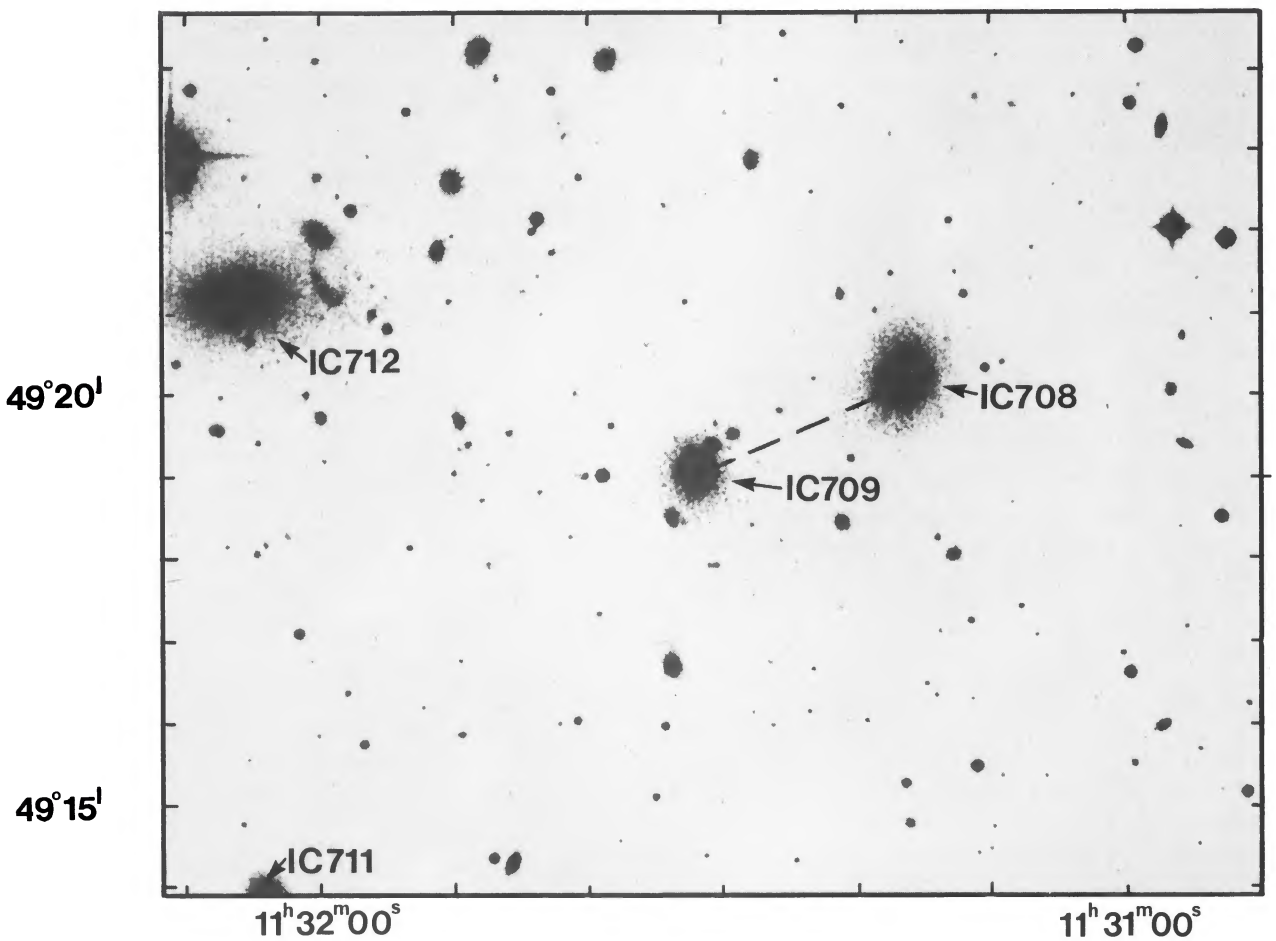

FIG. 6.—The cluster of galaxies Abell 1314 in the vicinity of IC 708, reproduced from a red-sensitive plate obtained with the 48 in Schmidt telescope at the Hale Observatories by Dr. A. G. de Bruyn and reproduced here with his kind permission. The cluster center is close to the position of IC 712 (see text, § IIIc).

starting values to guide the detailed numerical simulations described in § IV. We work throughout in center of mass coordinates.

1. The acceleration of IC 708 is

$$\ddot{\boldsymbol{r}}_1 = -\frac{G(m_1 + m_2)}{[1 + (m_1/m_2)]^3} \cdot \frac{\boldsymbol{r}_1}{r_1{}^3}, \tag{1}$$

where m_1 is the mass of IC 708, m_2 the mass of IC 709, and $\boldsymbol{r}_1$ the position vector of IC 708 with respect to the center of mass (e.g., Harwit 1973, eq. 3.19a). The equivalent mass at the center of mass is thus

$$M = \frac{m_1 + m_2}{[1 + (m_1/m_2)]^3}. \tag{2}$$

From the 0.8 mag difference in m_V between IC 708 and IC 709, $m_1/m_2 \sim 2.1$ if the two galaxies have the same mass to light ratio. Taking m_1 to be from 3×10^{12} to $3 \times 10^{13}\ M_\odot$ (Wilson and Vallée 1977) yields M in the range $1.5 \times 10^{11}\ M_\odot$ to $1.5 \times 10^{12}\ M_\odot$.

2. The radial velocity v_1 of IC 708 relative to the center of mass is

$$v_1 = \frac{\Delta v}{1 + (m_1/m_2)}, \tag{3}$$

where Δv is the observed difference in radial velocity between IC 708 and IC 709 (64 ± 210 km s^{-1}). For $m_1/m_2 = 2.1$, $v_1 = 21 \pm 68$ km s^{-1}.

3. From the definition of the center of mass,

$$l_1 = \frac{\Delta l}{1 + (m_1/m_2)}, \tag{4}$$

where l_1 and Δl are the projected distances on the sky between IC 708 and the center of mass and between IC 708 and IC 709 respectively. The observed value of $\Delta l = 145$ kpc then gives $l_1 = 47$ kpc (towards IC 709).

4. The projected distance l_1 must be less than $2a$, where a is the semimajor axis of IC 708's orbit around the center of mass, so $a > 24$ kpc.

© American Astronomical Society • Provided by the NASA Astrophysics Data System

1981ApJ...250...66V

5. Using Kepler's law, the orbital period

$$P = 3 \times 10^{12}\left(\frac{a}{\text{kpc}}\right)^{3/2}\left(\frac{M}{M_\odot}\right)^{-1/2} \text{ yr} \qquad (5)$$

which for $M = 1.5 \times 10^{11}\ M_\odot$ gives $P > 9 \times 10^8$ yr and for $M = 1.5 \times 10^{12}\ M_\odot$ gives $P > 3 \times 10^8$ yr.

6. The circular velocity

$$v_c = 2 \times 10^{-3}\left(\frac{a}{\text{kpc}}\right)^{-1/2}\left(\frac{M}{M_\odot}\right)^{1/2} \text{ km s}^{-1} \qquad (6)$$

is < 158 km s^{-1} for $M = 1.5 \times 10^{11}\ M_\odot$ and < 500 km s^{-1} for $M = 1.5 \times 10^{12}\ M_\odot$. As v_1 was only 21 ± 68 km s^{-1}, it is therefore likely that we are viewing IC 708 at a large angle to its spatial velocity. This conclusion could, however, be incorrect either if Δv is underestimated or if the orbit of IC 708 is highly eccentric and IC 708 is near its closest approach to the center of mass.

c) *The Cluster Center as the Attracting Center*

We have used positions for the galaxies in Abell 1314 privately communicated by Dr. A. Oemler to estimate that the cluster center is at 1950.0 coordinates $11^h32^m12^s \pm 12^s$, $+49°20' \pm 2'$. Sastry and Rood (1971) give the position of the cluster centroid as $11^h32^m06^s \pm 12^s$, $+49°20' \pm 2'$. The mean radial velocity of the 16 cluster members measured by Coleman *et al.* (1976) is $10{,}150 \pm 180$ km s^{-1}. We therefore surmise that the 15 mag galaxy IC 712 ($11^h32^m06^s.5 \pm 0^s.1$, $+49°21'16'' \pm 1''$, $v_r = 10{,}054$ km s^{-1}) may be resting at the cluster center to within the positional and velocity uncertainties. As the cluster center, or IC 712, can be a secondary center of attraction for IC 708 we have also constructed "double-orbit" models based on the assumption that IC 708 orbits both IC 709 and the cluster center. With this assumption the IC 708/709 pair describes an orbit in the cluster for which $l_1 \sim 460$ kpc and $v_1 \sim -570$ km s^{-1}. The distance traveled around the center of the cluster in 6×10^8 yr (a likely value for the period P of the "local" orbit of IC 708 around IC 709) is thus ~ 350 kpc, much larger than the probable size of the major axis ($2a > 47$ kpc) of the local orbit. For consistency with the observed shape of the trails, most of the distortion produced by the orbital motion around the cluster center must lie along the line of sight, which must therefore be almost tangent to the larger orbit. The assumption of the additional orbital motion about the cluster center does not directly improve the fit to the trail *shapes*, but it increases the fitted ejection velocities and decreases the time scales associated with the formation of the radio structure (see § V).

IV. DETAILED MODELS

We now compare the observed radio structure of IC 708 with detailed numerical simulations of an orbiting head-tail galaxy. The simulations have four main stages: (1) obtaining the shapes of the trail ridge lines in the planar case (Fig. 5*a*); (2) superposing on the planar structure the three-dimensional curvature resulting from the orbital motion of the galaxy; (3) imposing an assumed variation of radio emissivity with distance from the galactic nucleus throughout a finite volume around each ridge; and (4) projecting the resultant three-dimensional source model into a two-dimensional intensity map of specified resolution to simulate observations made from a specified line of sight. We now describe these steps in more detail.

a) *The Ridge Structure*

We adopt a Keplerian variation of the velocity $\boldsymbol{v}_g$ of the galaxy in magnitude and direction as in an elliptical orbit:

$$v_g^2 = GM \cdot \left(\frac{2}{r_1} - \frac{1}{a}\right). \qquad (7)$$

This provides both the twisting into three dimensions of the basic planar double trail shape (Fig. 5*b*) and a modification of the trail shape due to the variation of the space velocity $\boldsymbol{v}_0$ with which the matter is ejected into the trails. (This velocity is $\boldsymbol{v}_0 = \boldsymbol{v}_g + \boldsymbol{v}_e$, where $\boldsymbol{v}_e$ is the velocity of ejection of the trail material relative to the nucleus of the galaxy, which we assumed to be fixed in magnitude and direction). Variations in $\boldsymbol{v}_0$ around the orbit result in asymmetries between the two trails even if they would be completely symmetrical in the planar case (Fig. 5*a*).

To construct the ridge shapes we use equation (7) to find $\boldsymbol{v}_g$ (and hence $\boldsymbol{v}_0$) for successive positions of the galaxy, and then the appropriate trail-dynamics equation to find the distance from the galaxy traveled by the ejected material in the time between its ejection and the observation. We consider four models for the trail dynamics (eqs. 8 to 10 and the Appendix).

Jaffe and Perola (1973) (JP) obtained the relation

$$d = D[1 - \exp(-v_0 t/D)] \qquad (8)$$

for the separation d of trail material from a parent galaxy at time t following the hypersonic ejection of the material. The JP dynamics were derived for a gravitationless independent-blob model of 3C 129 and were later shown by Owen, Burns, and Rudnick (1978) to give a fair representation of the ridge shapes in the double trail structure of NGC 1265.

Cowie and McKee (1975) (CM) modified the JP independent-blob model, arguing that the ejection of the material should be only mildly supersonic with respect to the external medium. The cross sections of ejected plasmoids could then be treated as constant, as they are determined by the external thermal (not ram) pressure. In this "CM" model equation (8) must be replaced by

$$d = D \ln(1 + v_0 t/D), \qquad (9)$$

but otherwise the trail shapes are derived as before.

Blandford and Icke (1978) (BI) attributed the bending of the twin jets in 3C 31 to the acceleration experienced by the galaxy during a gravitational encounter with a near neighbor. In their model the trails are "heavy" jets which are neither decelerated nor bent by the ram pressure of the ICM; they are deviated by the "jerk" experienced by the galaxy near perigalacticon of its orbit. We have

© American Astronomical Society • Provided by the NASA Astrophysics Data System

1981ApJ...250...66V

reproduced the BI dynamics by replacing equation (8) with

$$d = v_0 t \,. \tag{10}$$

Begelman, Rees, and Blandford (1979) (BRB) presented a model of a continuous supersonic jet presumed to bend under the ram pressure of the ICM while maintaining a constant speed along a preestablished track. Their model also gave a fair representation of the ridge shapes in NGC 1265 provided that the jet is eventually disrupted and merges with shocked ICM when it travels at some critical angle to the line joining it to the stagnation point (where the jet is perpendicular to v_g). We derive the equation for the trail shape in the BRB dynamics in our Appendix, as it is given incorrectly in the original paper. We assume in our models that the trail material moves as described by equation (8) beyond the empirically determined "disruption point" of BRB.

b) *Construction of Intensity Maps*

Once the ridge shapes have been obtained, the emissivities of about 10^8 cells of side 1.5 kpc are calculated according to (1) the distance of the cell center from the nearest point on the ridge line and (2) the distance s of this point from the nucleus of the galaxy along the orbital path. Unfortunately, models of particle replenishment and magnetic field evolution in head-tail radio sources are not sufficiently developed to allow *a priori* predictions of the synchrotron emissivity variations along the trails. We are therefore forced to adopt simple analytic functions for the assumed radio emissivity variation $\epsilon(s)$. We have used $\epsilon = 0$ if the center of a cell is > 2.5 kpc from the ridge line and $\epsilon(s) = f(s/s_{\max})$ otherwise, where $s_{\max}$ is the total length of the radio trail measured along the path of the galaxy. We tried both exponential and Gaussian forms for f based on observed variations of intensity with distance along a number of well studied head-tail galaxies. The function $f(s/s_{\max})$ must in fact represent a more physically meaningful function of elapsed time $f'(t/t_{\max})$, but we are not concerned with the physics of the decrease in emissivity here. In particular, we seek to match only the large scale intensity variations along the trails in IC 708 to test the suitability of orbitally derived shapes for the structure and do not attempt to describe the intensity substructure or changes in width along its trails.

The map of the source obtained by a given observer is then calculated by projecting the three-dimensional array of emissivity cells onto two dimensions by a standard rotation of coordinates, assuming that the optical depth of the trails is negligible on all lines of sight through the structure. The resultant two-dimensional grid is smoothed to simulate a map at the resolution of the observations.

V. RESULTS

a) *Single-Orbit Models*

In the single-orbit models we adjust the orbital eccentricity, the length of the major axis, and the orientation of the orbit relative to the observer, as well as the assumed ejection velocity v_e and the stopping distance D (where relevant) to match both the large scale radio trail shapes of IC 708 and the optical data on IC 708/709, i.e. their relative radial velocity Δv, separation Δl, and position angle. We do not attempt to model the compact core source or the "blobby" substructure within the trails. In these models it is assumed that the ICM responsible for the bending of the trails is at rest with respect to the center of mass of IC 708 and IC 709—i.e., that it is a local "envelope" of gas around the two galaxies.

Figure 7 displays the most successful synthetic map of the trails obtained in 500 trials using the single-orbit hypothesis and equation (8) to define the trail shapes. The parameter set which produced this map is listed in the first row of Table 3. The differing lengths of the northern and southern trails between the radio core of IC 708 and the points A1 and A2 where they curve to form the hooks (see Fig. 7) are successfully reproduced in this model by the choice of the orientation of the observer relative to the orbit: the shorter southern trail is more nearly along the observer's line of sight. Although the emissivity ϵ was assumed to decrease with distance s along the trails as $\exp(-2s/s_{\max})$ in this model, the simulated map has local intensity maxima at B1 and B2 along the northern and southern trails. These maxima arise from a further projection effect, namely the increased lengths of the trails along the lines of sight as they curve around the past orbit of IC

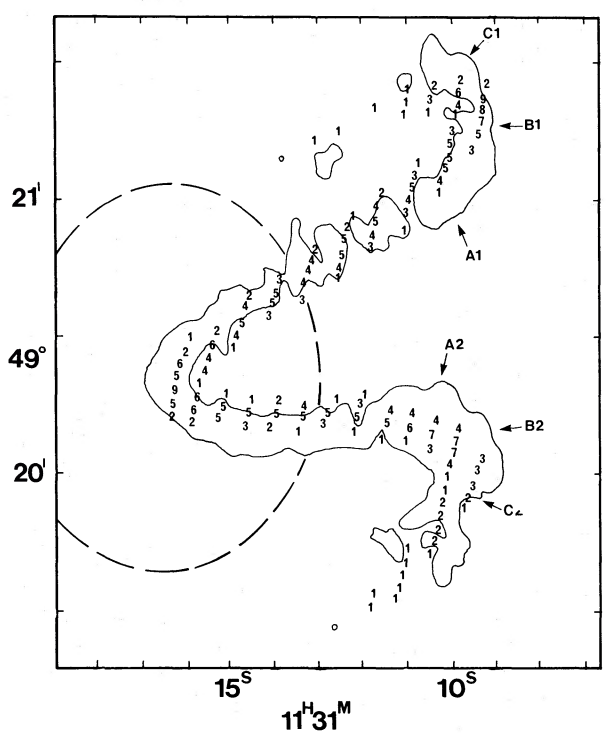

FIG. 7.—Simulated map of IC 708 in arbitrary intensity units, superposed on an outer contour of the VLA map shown in Fig. 3. The assumed orbital motion of IC 708 is a single orbit around the center of mass of IC 708/709; the dynamical model is that of Jaffe and Perola (1973), eq. (8) of the present text. Points *A*, *B*, and *C* are referred to in the text, § V*a*.

© American Astronomical Society • Provided by the NASA Astrophysics Data System

1981ApJ...250...66V

TABLE 3

PARAMETERS OF BEST-FITTING ORBITAL MODELS

Model Type (orbit type, dynamics)	Equivalent[a] Mass at Focus ($M_\odot$)	Eccentricity[a] Inclination (e, θ, ϕ)[b]	Semimajor[a] Axis (kpc)	Ejection Velocity (km s^{-1})	Stopping Distance (kpc)	Age at end of Trails (yr)	s_{max}[c] (kpc)
Single, JP	1×10^{10}	0.70, 336°, 3°	125	12	85	2×10^{10}	270
Single, CM	1×10^{10}	0.70, 336°, 3°	125	17	36	2×10^{10}	270
Single, BRB	1×10^{10}	0.70, 336°, 3°	125	550	80	6×10^{9}	160
Double,[d] JP	3.3×10^{11}	0.87, 354°, 89°	41	100	320	8×10^{8}	65
Double,[d] CM	3.3×10^{11}	0.87, 354°, 89°	41	85	270	1×10^{9}	86
Double,[d] BRB	3.3×10^{11}	0.87, 354°, 89°	41	7800	900	1×10^{8}	20

[a] Parameters in these columns refer to orbit of IC 708 about IC 708/709 center of mass.

[b] Angle θ: azimuth of line of sight from x-axis (in x-y plane); angle ϕ: polar angle of line of sight from z-axis (orbit of IC 708 around IC 708/709 center of mass is in x-z plane with its major axis parallel to z-axis).

[c] In all models, $\epsilon(s) = \exp(-2s/s_{max})$; see § V of text.

[d] Cluster orbit is assumed to be circular in double-orbit models.

708. The presence of similar intensity maxima in the data supports the basic interpretation of the source structure as arising from an orbital motion of IC 708. The large eccentricity ($e = 0.70$) of the orbit is needed in order to explain the lengths of the sections of the trails between points A1 and C1, and A2 and C2 on the northern and southern trails respectively. As the ejecta in these sections are highly decelerated by the ram pressure of the ICM, the lengths of A1 to C1 and A2 to C2 along the line of sight must significantly exceed the lengths from the radio core to A1 and A2, if the projected structure is to form "hooks" that are as open as those observed. These geometrical constraints can be satisfied only if the orbit is eccentric with the major axis oriented near the line of sight.

While the model shown in Figure 7 fits the shape of the hook structure far from IC 708 and the variation of intensity along the trails quite well, the modeled angle between the trails within 20″ of the core is clearly too small. No single-orbit model using equation (8) was found to fit this close-in structure better while retaining the fit to the "hooks." In effect, the trails in IC 708 appear to separate more rapidly near the galaxy, and less rapidly further away, than would be predicted by equation (8). Furthermore, the ejection velocities required by the model's dynamics are very low (a few tens of km s^{-1}) in all models that gave reasonable fits to the data.

Such low velocities raise at least three serious objections to the dynamical basis of such models. First, the deduced ages of the material at the ends of the trails are so high (of the order of the Hubble time) that the assumption that IC 708 and IC 709 have remained a closed dynamical system over the lifetime of the radio source is untenable. Second, the low ejection velocities cannot be hypersonic, as the model assumed. Third, at such low ejection velocities the assumption that the trajectory of the material would be unaffected by gravitation cannot be maintained.

We therefore regard the model shown in Figure 7 as a useful demonstration of the ability of an orbitally derived *shape* to reproduce the observed radio map, but we find its underlying dynamics to be unacceptable. Guided by the orbital parameters which simulate the trail shapes successfully in this model, we made further models using the CM dynamics embodied in equation (9). The best-fitting CM models differed only in minor details from those obtained using equation (8); the parameters of the best fit obtained in 30 trials are given in row 2 of Table 3. Single-orbit models based on equation (9) are therefore subject to the first and third objections made above to the JP models. We therefore also reject these models.

All attempts to simulate the observed structure using the BI "heavy jet" dynamics failed completely to reproduce the outer (hooked) half of the trails, showing that the ICM must in fact strongly decelerate material ejected from IC 708, in contrast to the hypotheses implicit in the BI dynamics.

We achieved most success in fitting single-orbit models to the observations using the continuous-jet dynamics given in the Appendix, with JP dynamics describing the motion of the material beyond the empirically determined "disruption point" where the jet is presumed by Begelman, Rees, and Blandford (1979) to share its momentum with shocked ICM. Although the implied age of the particles at the ends of the trails is significantly reduced in the best-fitting model of this kind (Table 3, row 3), it remains very long (6×10^9 yrs). We must still have serious reservations about the assumption of dynamical isolation of the IC 708/709 system over such a time scale. Furthermore, this model "particle age" is much longer than the expected radiative lifetime (3×10^7 yrs) of particles emitting at 4.9 GHz in the equipartition magnetic field of the trails and in the equivalent magnetic field of the 2.7 K background.

This time scale problem in the single-orbit models arises primarily from the apparently small difference in radial velocities, $\Delta v = 64 \pm 210$ km s^{-1}, between IC 708 and IC 709. Unless the uncertainties in the two radial velocities are utilized to postulate $\Delta v \gg 64$ km s^{-1}, low ejection velocities are required in order to obtain the observed trail curvature; these in turn lead to large "ages" for the ends of the trails. We therefore conclude that unless the true radial velocity difference between IC

© American Astronomical Society • Provided by the NASA Astrophysics Data System

1981ApJ...250...66V

708 and IC 709 significantly exceeds 64 km s^{-1}, all single-orbit models for the trails of IC 708 must be rejected on the basis of their excessively long time scales.

The equivalent barycentric mass M required by the single-orbit models is also significantly less than that estimated in § III*b*. The observed shape of the two ridges constrains r_1 in equation (7) to be small, because in the single-orbit model IC 708 must be approaching perigalacticon. We must also be observing close to the major axis of the orbit to obtain the correct shape for the hook structure. This requires $v_r \sim v_g$, so that v_g must also be small in equation (7). The small resulting value of M ($\sim 10^{10}\ M_\odot$) represents a further contradiction between the single-orbit models and reasonable expectations for the dynamics of the IC 708/709 system.

b) *Double-Orbit Models*

The constraints which lead us to reject single-orbit models can be removed in double-orbit models to some extent, because of the $\sim$ 570 km s^{-1} difference in radial velocity between IC 708/709 and the cluster mean. If we assume that IC 708 orbits IC 709 while also moving through an ICM that is stationary with respect to the cluster center, more plausible models can be constructed.

In these double-orbit models, not only the trail shapes and intensities but also five optical data are fitted: the separation of IC 708 from IC 709, the separation of IC 708 from the cluster center (presumed to lie at IC 712 [§ III*c*]), the difference in position angle between these two separation vectors, and the radial velocities of IC 708 and IC 709 relative to the cluster mean. The models are constructed by first finding the contributions of the "local" and "cluster" orbits to v_g and then adding these vectorially for insertion into the dynamical equations. For simplicity, we assume that the larger scale "cluster" orbit is circular. (As the observed trail represents only a small fraction of the length of this orbit, our results are not sensitive to the eccentricity, if any, of this orbit).

The best-fitting double-orbit models based on JP and CM dynamics (Table 3, rows 4 and 5) again failed to simulate both the inner and outer trail shapes simultaneously. Furthermore, the time scales associated with the ends of the trails in these models remain high ($\sim 10^9$ yrs) even in the double-orbit context. Trials using the "heavy jet" BI dynamics again failed completely to reproduce the outer half of the observed structure.

The most successful double-orbit simulations were those based on the continuous-jet dynamics of the Appendix. The best-fitting synthetic map obtained in 300 trials is shown in Figure 8, and the corresponding model parameters are listed in Table 3, row 6. This model fits both the inner and outer trail shapes well, while retaining an acceptable fit to the distribution of intensity along the trails (Fig. 9). It must of course be borne in mind that the model has the flexibility of choosing an *empirical* point along the trails to be the "disruption point" where the dynamics of the ejecta revert to JP dynamics. This is at least partly responsible for the improvement in the fit to the trail shapes in comparison to the model displayed in Figure 7.

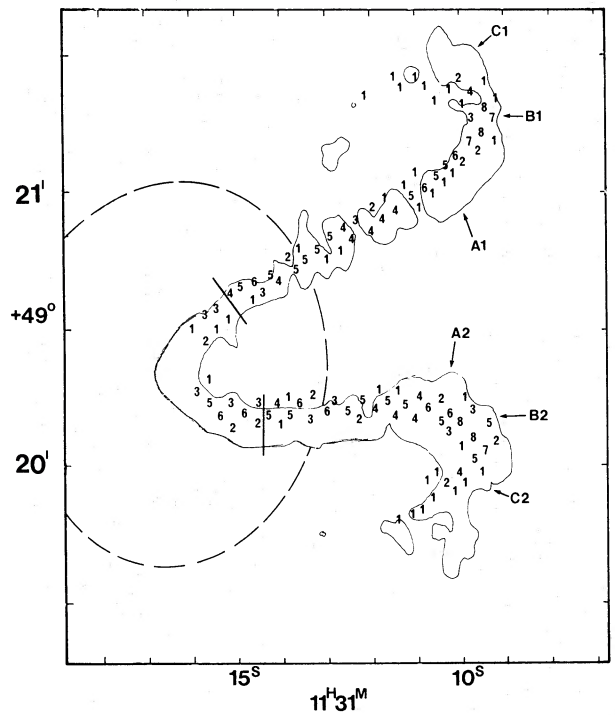

FIG. 8.—Simulated map of IC 708 in arbitrary intensity units, superposed on an outer contour of the VLA map shown in Fig. 3. The assumed orbital motion of IC 708 is a double orbit around the center of mass of IC 708/709 and around the center of Abell 1314; the dynamical model is that of the Appendix out to the "disruption points" (marked by ticks), followed by Jaffe-Perola dynamics further from the galaxy. This map shows the most satisfactory fit obtained to the observed structure of IC 708 (see text, § V*b*).

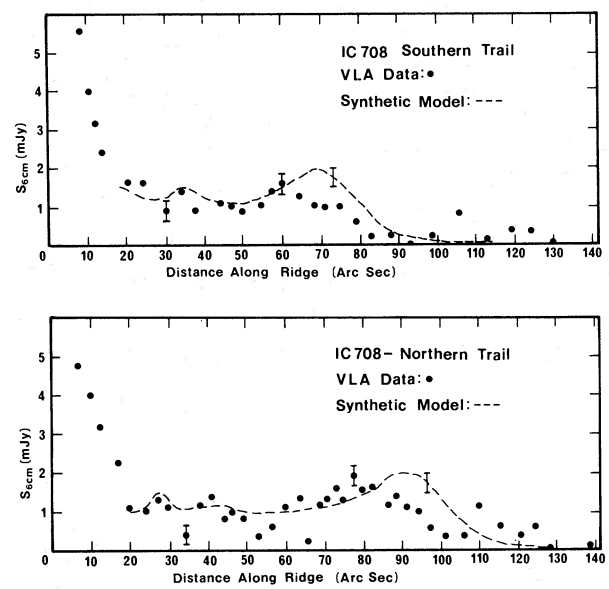

FIG. 9.—Comparison of observed and simulated intensity distributions along the ridge lines of the trails, from Fig. 8. The data decrease in brightness faster than the model, due mainly to our choice of a constant width trail for modeling purposes; the actual trail width increases with distance from IC 708 (see § II*c*).

© American Astronomical Society • Provided by the NASA Astrophysics Data System

1981ApJ...250...66V

The modeled ejection velocity of 7800 km s^{-1} and the required critical angle of 87° for disruption of the jets are similar to those of 10^4 km s^{-1} and 75° derived by Begelman, Rees, and Blandford (1979) for their fit to the structure of NGC 1265. In both cases the large values of the critical angle require that the jets be remarkably stable against disruption by their interaction with the ICM through which the parent galaxy is traveling.

The age of the ends of the trails in this model is 10^8 yrs. While this is still somewhat longer than the radiative lifetime of 3×10^7 yrs for the electrons emitting at 4.89 GHz in the equipartition magnetic field, the discrepancy is no longer as serious as in the other double-orbit models and in all single-orbit models. Observations of the distribution of the radio spectral index over the trail structure are necessary in order to establish how serious a constraint the remaining time scale discrepancy actually places on the continuous-jet interpretation. The radial velocities of IC 708 and IC 709 should also be redetermined with greater precision, for a velocity difference $\Delta v > 64$ km s^{-1} would assist in removing the time scale problem (if any) from this model.

The double-orbit model also removes the constraints on the barycentric mass M discussed at the end of § V*a* and leads to estimates of $M \sim 3.3 \times 10^{11}\ M_\odot$ (Table 3) that are more consistent with our initial expectations for this parameter (§ III*b*).

VI. CONCLUSIONS

Orbital models of the trail structure of IC 708 appear to be attractive provided (1) that the orbital velocities significantly exceed the small radial velocity difference between IC 708 and IC 709, and (2) that continuous-jet dynamics are employed to describe the motions of the radio ejecta. The orbital models avoid the need to invoke asymmetric diffusion of relativistic particles perpendicular to the motion of IC 708 in order to explain the radio "wings" (cf. Vallée, Wilson, and van der Laan 1979). The broad intensity maxima near the beginnings of the hooked structures can also be explained by the same projection effects that account for the asymmetries between the trails. The basic geometry of the orbital models therefore offers a simple explanation for several of the major features of the radio structure of IC 708. Double-orbit models, while having the unpleasant aspect of larger numbers of adjustable parameters, provide a plausible means of satisfying the velocity (and time scale) constraints required for an acceptable description of the source.

The fact that continuous-jet dynamics appear to be required in order to fit the trail *shapes* reinforces the analogies drawn directly from the maps in § II between the intensity and polarization distributions over IC 708 and over the straight jets in 3C 31, NGC 315, and 3C 449. The one-sidedness of the high brightness features within ~ 2 kpc of the radio core, the probable orientation of the magnetic field parallel to the extension of these features, and the subsequent transition to a predominantly perpendicular orientation further from the core, all resemble observed features of straight jets in low luminosity radio galaxies. Our results strongly suggest that in IC 708 we are viewing a system intrinsically similar to the low luminosity "twin-jet" radio galaxies, but whose jets are bending backwards into a **U**-shape without significant modification of their internal structure. These observations therefore add to the growing body of evidence for the stability of large scale supersonic jets against disruption by external pressures or by the growth of internal perturbations, even while bending through angles approaching 90° due to interactions with the ICM.

Finally, we note that high resolution radio observations may now be able to contribute to studies of galaxy-galaxy interactions by identifying galaxies whose radio structures exhibit the effects of gravitational encounters. Orbital parameters have now been suggested for 3C 129, NGC 4874, 3C 31, and IC 708 on the basis of radio structural data. These putative "binary galaxies" are situated at the long period end of the period distribution for such systems and extend the range that can be sampled by optical observations alone.

We thank Drs. R. C. Bignell and F. N. Owen, and the staff of the VLA, for their help and cooperation during the observations and their reduction. We also thank Dr. R. N. Henriksen for many discussions of jet dynamics and Dr. M. J. L. Kesteven for advice on map simulation using the Astronomy Computing Facility at Queen's University. This research was supported by grants to A. H. B. from the Natural Sciences and Engineering Research Council of Canada (NSERC), and to the Astronomy Computing Facility from NSERC, from the Advisory Research Committee and from the Department of Physics at Queen's University.

A. H. B. also thanks the National Radio Astronomy Observatory and the University of New Mexico for their hospitality during a sabbatical leave in which this work was completed.

APPENDIX

CONTINUOUS JET DYNAMICS

If the flow along the trail approximates a constant speed (v_e) jet of scale height h transverse to the flow direction, and if the flow is mass-conserving and adiabatic we will have

$$\rho_j h^2 = \text{constant} \quad \text{and} \quad p_j \propto \rho_j^{\Gamma} \propto h^{-2\Gamma}\,, \tag{A1}$$

© American Astronomical Society • Provided by the NASA Astrophysics Data System

1981ApJ...250...66V

where ρ_j and p_j are the jet density and pressure respectively and Γ is the adiabatic index.

It the galaxy moves supersonically, there will be a cylindrical standoff shock in the ICM ahead of the galaxy, and the pressure at the stagnation point where the jet is perpendicular to $\boldsymbol{v}_g$ will exceed that in the ambient ICM by an amount p_0. The excess pressure on the jet at a point where the surface normal to the jet makes an angle ϕ to the surface normal at the stagnation point will be $p \sim p_0 \cos^2 \phi$.

Following Begelman, Rees, and Blandford (1979) we take coordinates X inward normal to the jet and Y tangent to the jet at the stagnation point. We also write $Y' = dY/dX$ and $Y'' = d^2Y/dX^2$. Then $\cos^2 \phi = Y'^2/(1 + Y'^2)$ and the radius of curvature R_j of the jet is

$$R_j = \frac{(1 + Y'^2)^{3/2}}{Y''} . \tag{A2}$$

If $p \sim p_j$, we also have

$$\frac{p}{p_0} \sim \left(\frac{h}{h_0}\right)^{-2\Gamma} \sim \frac{Y'^2}{1 + Y'^2} , \qquad \text{i.e., } h = h_0\left(\frac{1 + Y'^2}{Y'^2}\right)^{1/2\Gamma} . \tag{A3}$$

The effective acceleration g felt by the jet material as it follows its curved path can be written

$$g = v_e{}^2/R_j = v_e{}^2 Y''(1 + Y'^2)^{-3/2} , \tag{A4}$$

and this must be provided by the ram pressure per unit length per unit mass of jet material:

$$g = -p/\rho_j h = -p_0 \cos^2\phi(h/\rho_{j0} h_0{}^2) . \tag{A5}$$

From equations (A4) and (A5) it follows that

$$v_e{}^2 Y''(1 + Y'^2)^{-3/2} = -\left(\frac{p_0}{\rho_{j0} h_0}\right)\left(\frac{1 + Y'^2}{Y'^2}\right)^{(1-2\Gamma)/2\Gamma} , \tag{A6}$$

so that we can write

$$Y'' = -\left(\frac{p_0}{\rho_{j0} h_0 v_e{}^2}\right) \cdot (1 + Y'^2)^{(1+\Gamma)/2\Gamma} \cdot Y'^{(2\Gamma-1)/\Gamma} . \tag{A7}$$

Our equations (A3) and (A7) differ from those of Begelman, Rees, and Blandford (1979) by the factors Y'^2 in the denominators on their right-hand sides, presumably due to typographical errors in the published version of their paper. Integration of equation (A7) gives the (X, Y) locations of the jet material; in our orbital models we have allowed for variations of $\boldsymbol{v}_g$ in integrating equation (A7), by putting

$$p_0 \propto \rho_0 v_g{}^2 .$$

Integration of equation (A7) locates the ejecta in the plane containing $\boldsymbol{v}_e$ and $\boldsymbol{v}_g$; this location is transformed to (x_m, y_m, z_m) by a standard coordinate transformation.

In applying these equations we have taken $\Gamma = \frac{5}{3}$ throughout.

REFERENCES

Begelman, M. C., Rees, M. J., and Blandford, R. D. 1979, *Nature*, **279**, 770 (BRB).
Blandford, R. D., and Icke, V. 1978, *M.N.R.A.S.*, **185**, 527 (BI).
Burns, J. O., Owen, F. N., and Rudnick, L. 1979, *A.J.*, **84**, 1683.
Byrd, G. G., and Valtonen, M. J. 1978, *Ap. J.*, **221**, 481.
Coleman, G. D., Hintzen, P., Scott, J. S., and Tarenghi, M. 1976, *Nature*, **262**, 476.
Cowie, L. L., and McKee, C. F. 1975. *Astr. Ap.*, **43**, 337 (CM).
de Vaucouleurs, G., and Nieto, J.-L. 1979, *Ap. J.*, **231**, 364.
Ekers, R. D., Fanti, R., Lari, C., and Parma, P. 1978, *Nature*, **276**, 588.
Fomalont, E. B., Bridle, A. H., Willis, A. G., and Perley, R. A. 1980, *Ap. J.*, **237**, 418.
Gisler, G. R. 1976, *Astr. Ap.*, **51**, 137.
Harwit, M. 1973, *Astrophysical Concepts* (New York: J. Wiley & Sons), p. 79.
Haslam, C. G., Kronberg, P. P., Waldthausen, H., Wielebinski, R., and Schallwich, D. (1978), *Astr. Ap. Suppl.*, **31**, 99.
Högbom, J. A. 1974, *Astr. Ap. Suppl.*, **15**, 417.
Hunt, R. 1971, *M.N.R.A.S.*, **154**, 141.
———. 1979, *M.N.R.A.S.*, **188**, 83.
Jaffe, W. J., and Perola, G. C. 1973, *Astr. Ap.*, **26**, 423 (JP).
Jaffe, W. J., Perola, G. C., and Valentijn, E. A. 1976, *Astr. Ap.*, **49**, 179.
Lea, S. M., and De Young, D. S. 1976, *Ap. J.*, **210**, 647.
Miley, G. K. 1980, *Ann. Rev. Astr. Ap.*, **18**, 165.
Miley, G. K., Perola, G. C., van der Kruit, P. C., and van der Laan, H. 1972, *Nature*, **237**, 269.
Miley, G. K., Wellington, K. J., and van der Laan, H. 1975, *Astr. Ap.*, **38**, 381.
Owen, F. N., Burns, J. O., and Rudnick, L. 1978, *Ap. J.* (*Letters*), **226**, L119.
Owen, F. N., Hardee, P. E., and Bignell, R. C. 1980, *Ap. J.* (*Letters*), **239**, L11.
Owen, F. N., and Rudnick, L. 1976, *Ap. J.* (*Letters*), **205**, L1.
Perley, R. A., Willis, A. G., and Scott, J. S. 1979, *Nature*, **281**, 437.
Readhead, A. C. S., Pearson, T. J., Cohen, M. H., Ewing, M. S., and Moffet, A. T. 1979, *Ap. J.*, **231**, 299.

© American Astronomical Society • Provided by the NASA Astrophysics Data System

1981ApJ...250...66V

Sastry, G., and Rood, H. 1971, *Ap. J. Suppl.*, **23**, 371.
Thompson, A. R., Clark, B. G., Wade, C. M., and Napier, P. J. 1980, *Ap. J. Suppl.*, **44**, 151.
Turland, B. D. 1975, *M.N.R.A.S.*, **170**, 281.
Vallée, J. P. 1977, *J.R.A.S. Canada*, **71**, 443.
Vallée, J. P., and Wilson, A. S. 1976, *Nature*, **259**, 451.
Vallée, J. P., Wilson, A. S., and van der Laan, H. 1979, *Astr. Ap.*, **77**, 183.
Valtonen, M. J., and Byrd, G. G. 1979, *Ap. J.*, **230**, 655.
Wilkinson, P. N., Readhead, A. C. S., Purcell, G. H., and Anderson, B. 1977, *Nature*, **269**, 764.
Wilson, A. S., and Vallée, J. P. 1977, *Astr. Ap.*, **58**, 79.
Zwicky, F., and Herzog, E. 1966, *Catalogue of Galaxies and of Clusters of Galaxies*, Vol. **3** (Pasadena: California Institute of Technology).

A. H. BRIDLE: National Radio Astronomy Observatory, VLA Program, P. O. Box O, Socorro, NM 87801

J. P. VALLÉE: Herzberg Institute of Astrophysics, National Research Council of Canada, 100 Sussex Drive, Ottawa, Ont. K1A 0R6, Canada

A. S. WILSON: Astronomy Program, University of Maryland, College Park, MD 20742

© American Astronomical Society • Provided by the NASA Astrophysics Data System